Electronic supplementary information

Band gap evolution and piezoelectric-to-electrostrictive crossover in (1-x)$KNbO_3$-x$(Ba_{0.5}Bi_{0.5})(Nb_{0.5}Zn_{0.5})O_3$ ceramics

Cristina Pascual-Gonzalez[a], Giorgio Schileo[b], Amir Khesro[b], Iasmi Sterianou[a], Dawei Wang[b], Ian M. Reaney[b], Antonio Feteira[a]

a. Christian Doppler Lab on Advanced Ferroic Oxides, Materials and Engineering Research Institute, Sheffield Hallam University, Howard Street, S1 1WB, Sheffield, United Kingdom
b. Department of Materials Engineering and Science, The University of Sheffield, S1 4JD, Sheffield, United Kingdom

Corresponding author: Antonio Feteira, email: a.feteira@shu.ac.uk

Prior to synthesis of the (1−*x*)$KNbO_3$-*x*$(Ba_{1/2}Bi_{1/2})(Zn_{1/2}Nb_{1/2})O_3$ (KBBNZ) series, stoichiometric $KNbO_3$ and K-deficient $K_{0.95}NbO_3$ samples were prepared in order to evaluate the impact of an eventual K volatilisation during the high temperature processing. All associated results are given in this ESI and hereafter one summarises the main findings in terms of purity, crystal structure, stability and band gap. From the XRD analysis (ESI, Fig. S1), the stoichiometric $KNbO_3$ sample appears to be single-phase within the detection limits of the technique, whereas K-deficient $K_{0.95}NbO_3$ sample exhibits the presence of $K_4Nb_6O_{17}$ as a secondary phase, which is highly hygroscopic a leads to the rapid disintegration of the ceramics by immersion in water (ESI, Fig. S2). In terms of microstructures, K-deficient $K_{0.95}NbO_3$ ceramics exhibit finer grains sizes (ESI, Fig. S3). Concerning vibrational and optical properties, both samples exhibit similar Raman spectra (ESI, Fig. S4) and indirect band gaps with values around 3.2 eV (ESI, Fig. S5), which is in broad agreement with the literature. The indirect band gaps for all KN-BBZN ceramics are listed in Table II. In summary, it can be anticipated that under the chosen processing conditions the loss of K can be considered negligible. Hence, no excess K was employed in the subsequent synthesis of the KN-BBNZ series. Dense KN-BBNZ ceramics are revealed by the SEM images (ESI, Fig. S6). Grain size appears to increase with increasing x. No secondary phases are detected. *In-situ* Raman spectroscopy clearly reveals the occurrence of three structural phase transitions in ferroelectric $KNbO_3$ ceramics (ESI, Fig. S7a), but also shows that those transitions do not occur in the non-ferroelectric KN-BBNZ x=0.25 ceramics (ESI, Fig. S7b). Temperature dependent measurements of the permittivity in function of the frequency were carried out (ESI, Fig. S8). KN (x=0) shows a room-temperature ε_r of ~300, as shown in Fig. S8a. A strong frequency dependence of both ε_r and tan θ is observed for x=0.05 and 0.10, as illustrated in Fig. S8b and S8c, respectively. The temperature for the ε_r anomalies remains almost unaltered, but it magnitude decreases with increasing frequency. For $x \geq 0.15$ the frequency dependence is much less pronounced, as shown in Fig. S8d and S8e. The compositional variation of the electric field-induced strain with the spontaneous polarisation for KN-BBNZ ceramics shows a good correlation (ESI, Fig. S9). The variation of the strain with P^2 was employed to estimate the electrostrictive coefficients, Q of KN-BBNZ x=0.05-0.20 (ESI, Fig. S10). Finally, the temperature dependence of the unipolar strain of KN-BBNZ x=0.05 measured at 50 kV/cm, shows a gradual but moderate (~14%) decrease with increasing temperature (ESI, Fig. S11).

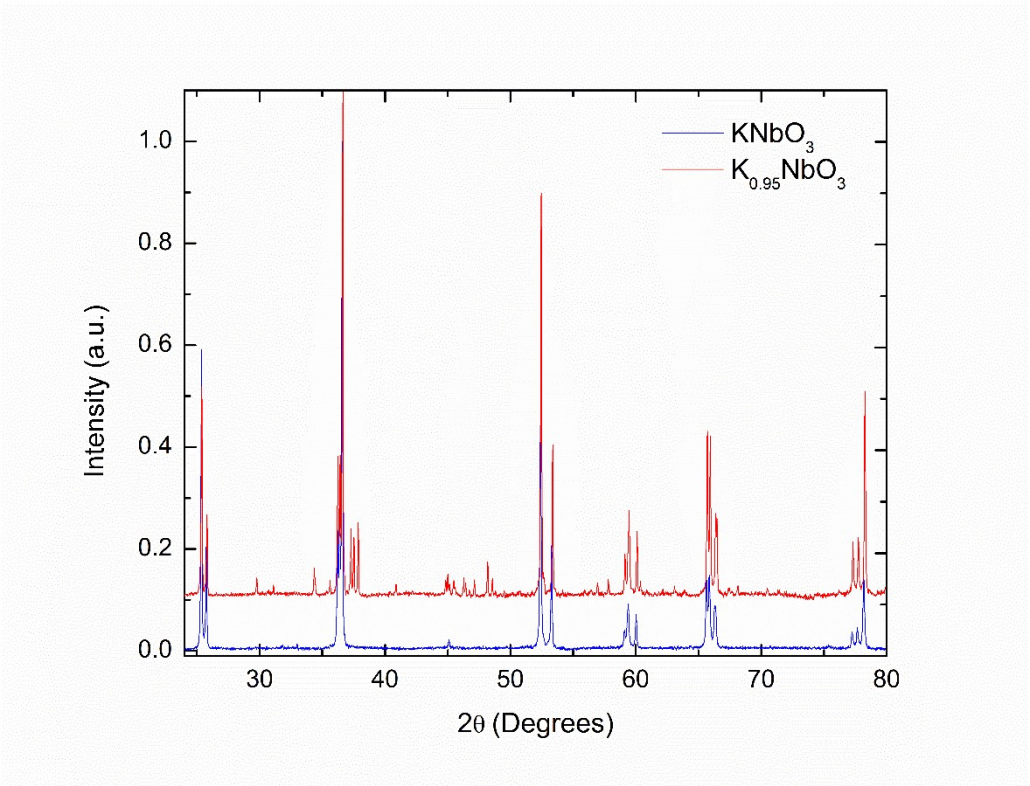

Figure S1. Room-temperature XRD data for (bottom) virtually pure stoichiometric $KNbO_3$ ceramics and (top) $K_{0.95}NbO_3$ ceramics containing $K_4Nb_6O_{17}$ as a secondary phase.

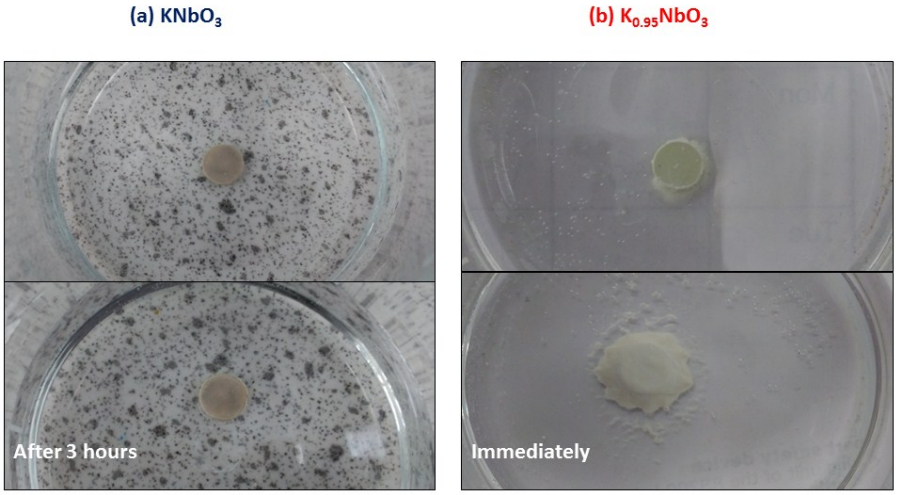

Figure S2. (a) $KNbO_3$ ceramics demonstrated no reaction under water even after 3 hours. (b) $K_{0.95}NbO_3$ ceramics when immersed in water, they immediately demonstrated a highly hygroscopic behaviour; i.e. the sintered bodies showed a quick disintegration and dissolved into water. The surrounding water got muddy at the same time.

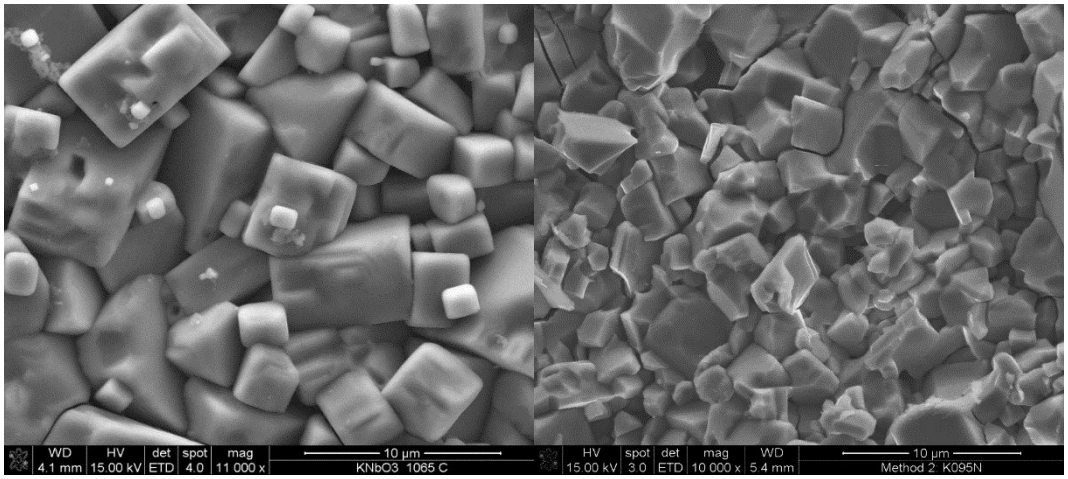

Figure S3. Microstructures for (left) stoichiometric $KNbO_3$ ceramics and (right) $K_{0.95}NbO_3$ ceramics.

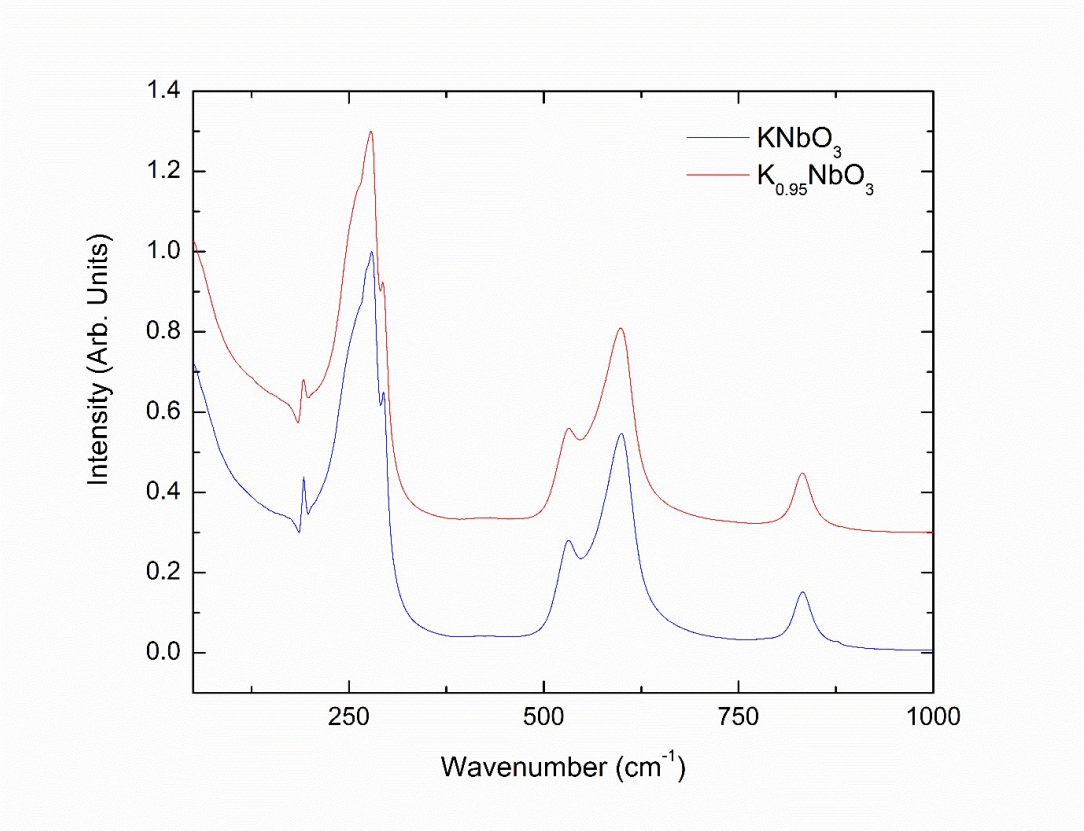

Figure S4. Room-temperature Raman data for (bottom) virtually pure stoichiometric $KNbO_3$ ceramics and (top) $K_{0.95}NbO_3$ ceramics.

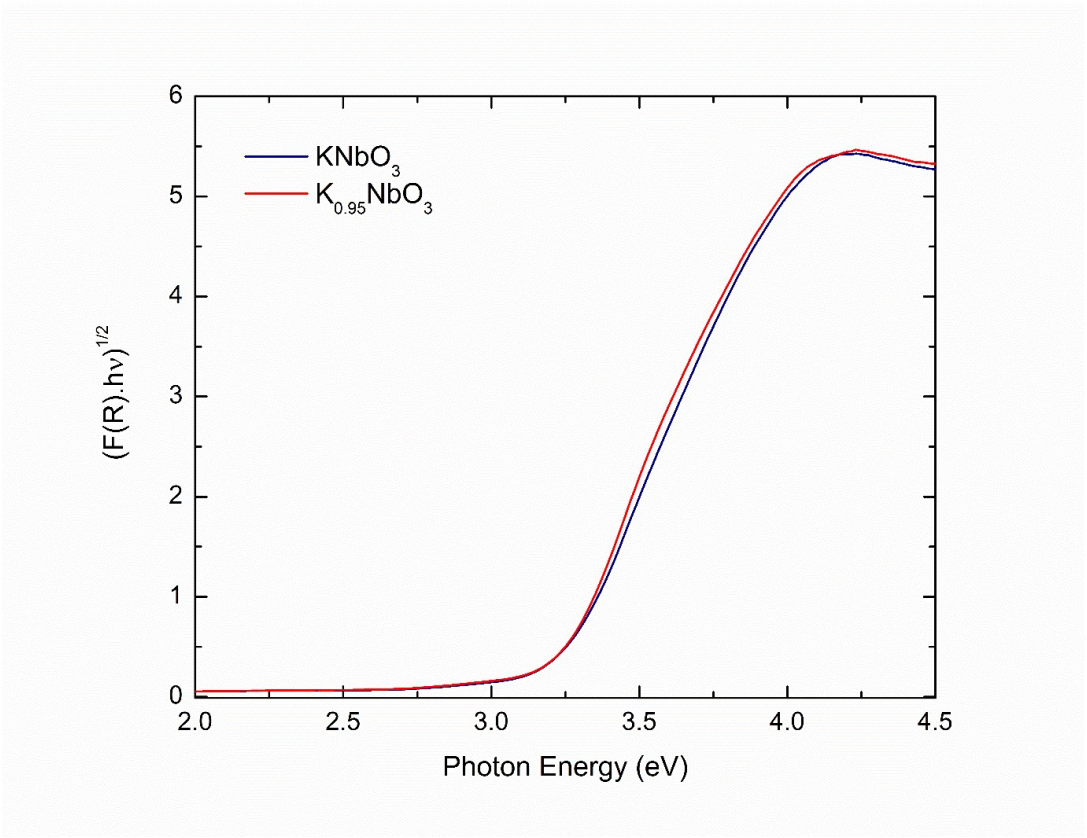

Figure S5. Tauc's plot for (bottom) virtually pure stoichiometric $KNbO_3$ ceramics and (top) $K_{0.95}NbO_3$ ceramics showing that both have similar band gaps ~3.2 eV.

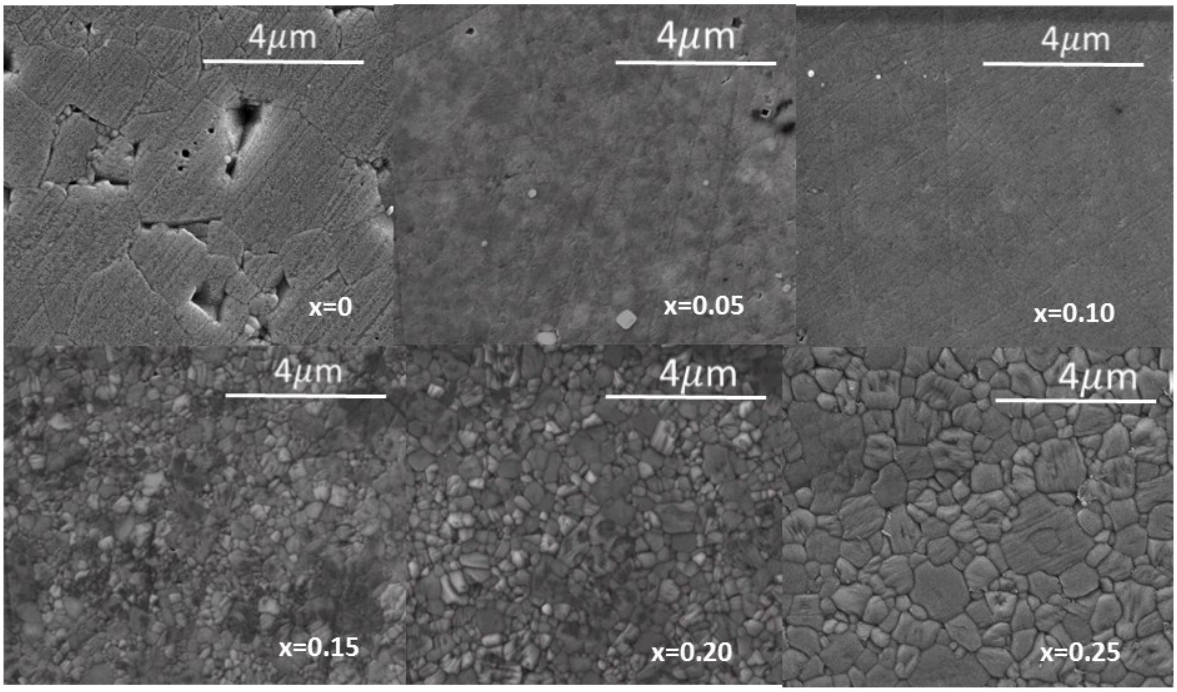

Figure S6. Microstructures for KN-BBNZ (0≤ x≤ 0.25) ceramics showing initially a grain size reduction with doping, which is followed by a gradual increase in grain size as x increases.

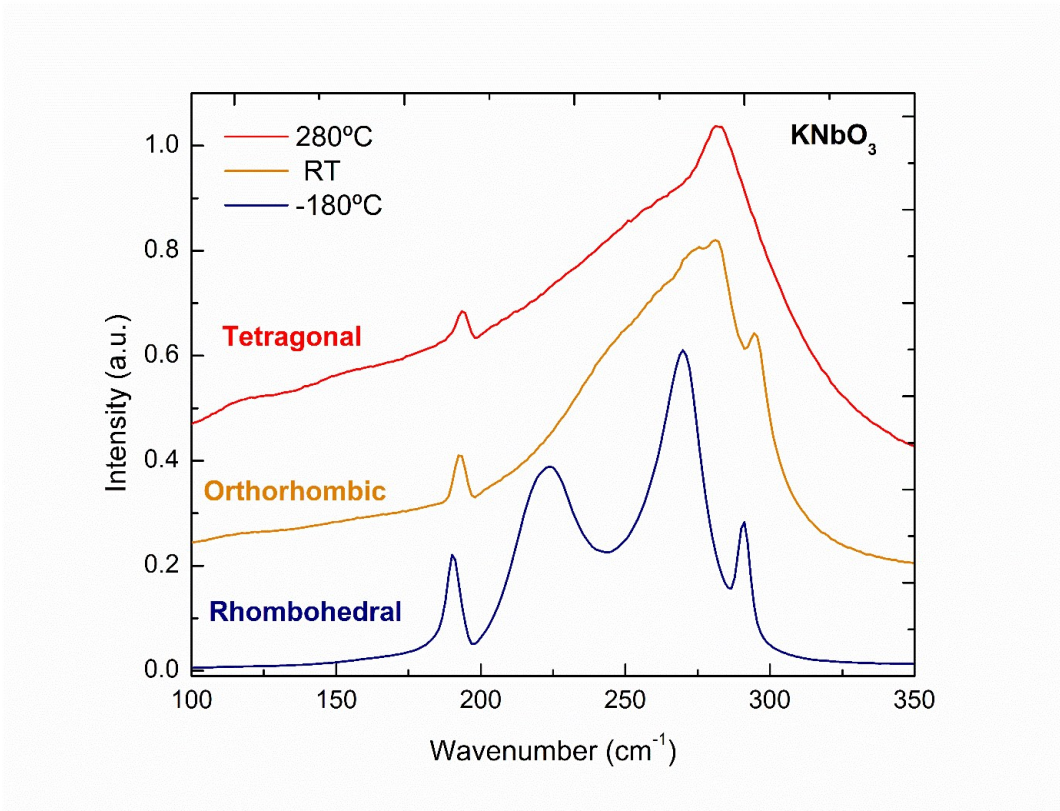

Figure S7a. In-situ Raman for $KNbO_3$ showing the typical spectrum for each of the three ferroelectric polymorphs. The sharp modes are regarded as "fingerprints" for ferroelectricity. Data corrected with the Bose-Einstein factor.

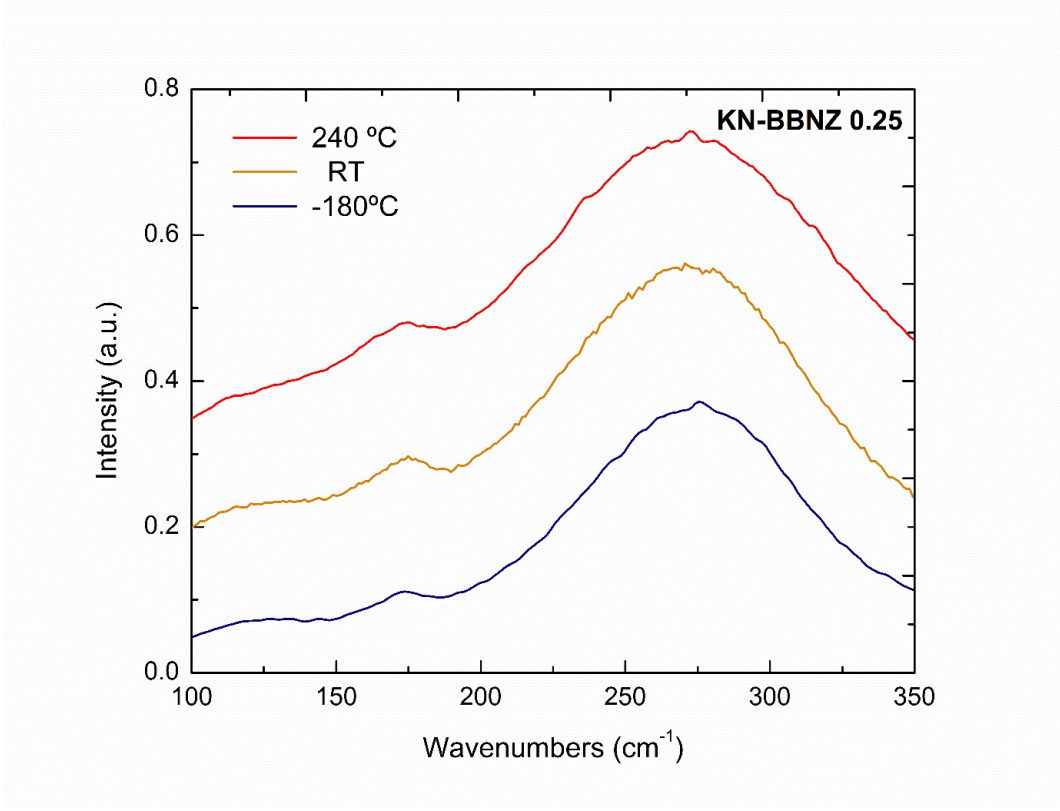

Figure S7b. In-situ Raman for KN-BBNZ X=0.25, showing both the absence of structural phase transitions and of sharp modes associated to the occurrence of ferroelectricity. Data corrected with the Bose-Einstein factor.

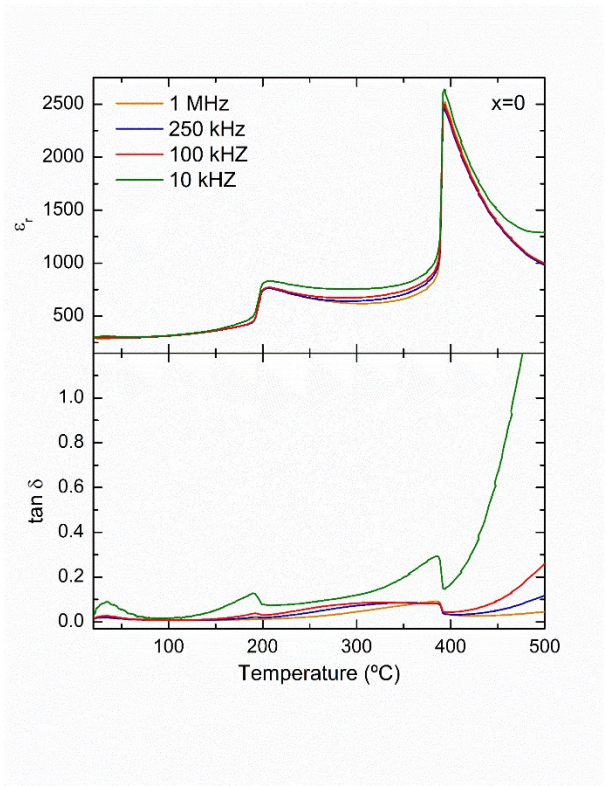

Figure S8a. Temperature dependence of ε_r and tan θ for KN ceramics.

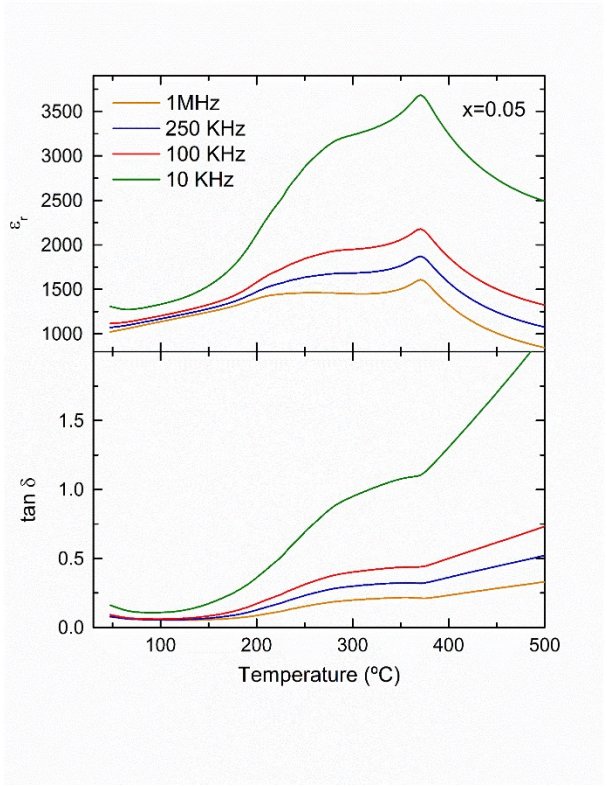

Figure S8b. Temperature dependence of ε_r and tan θ for KN-BBZN x=0.05 ceramics.

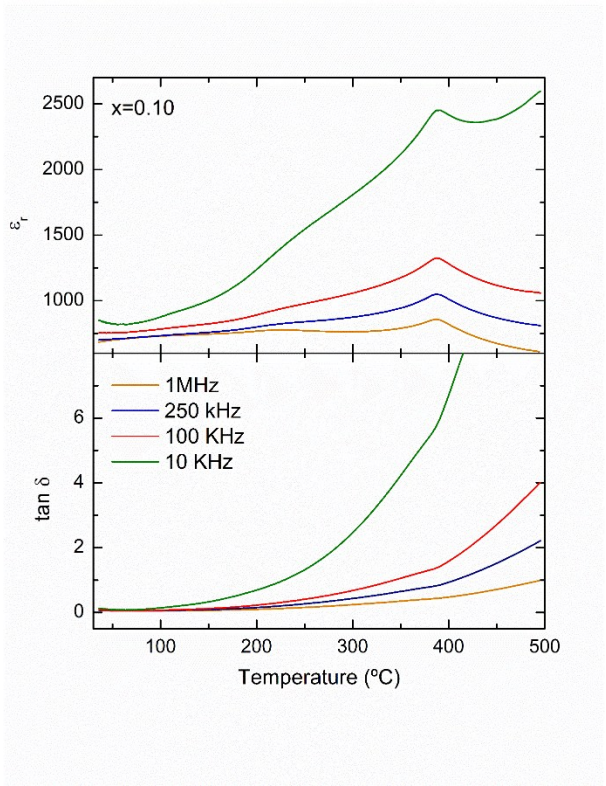

Figure S8c. Temperature dependence of ε_r and tan θ for KN-BBZN x=0.10 ceramics.

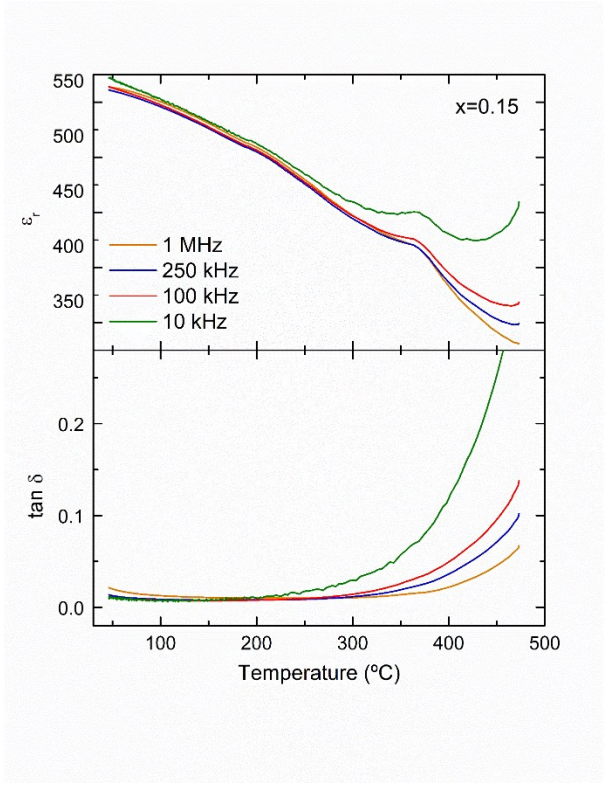

Figure S8d. Temperature dependence of ε_r and tan θ for KN-BBZN x=0.15 ceramics.

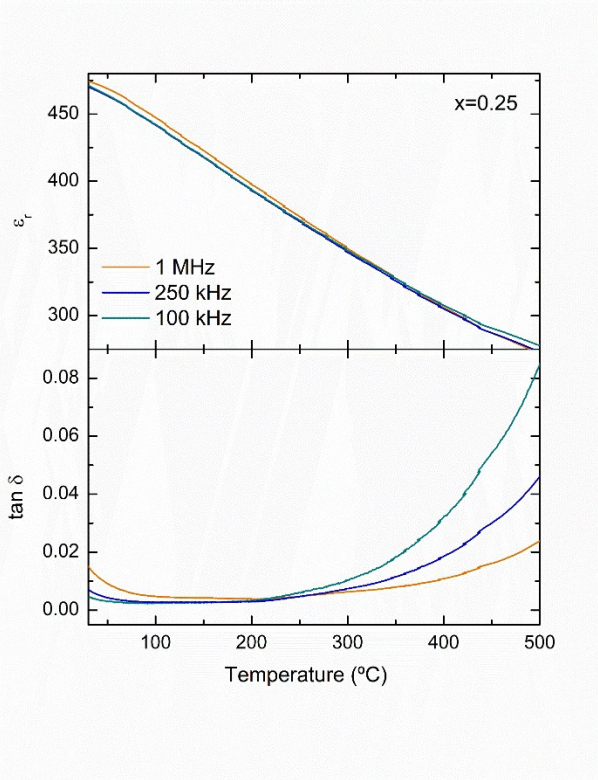

Figure S8e. Temperature dependence of ε_r and tan θ for KN-BBZN x=0.25 ceramics.

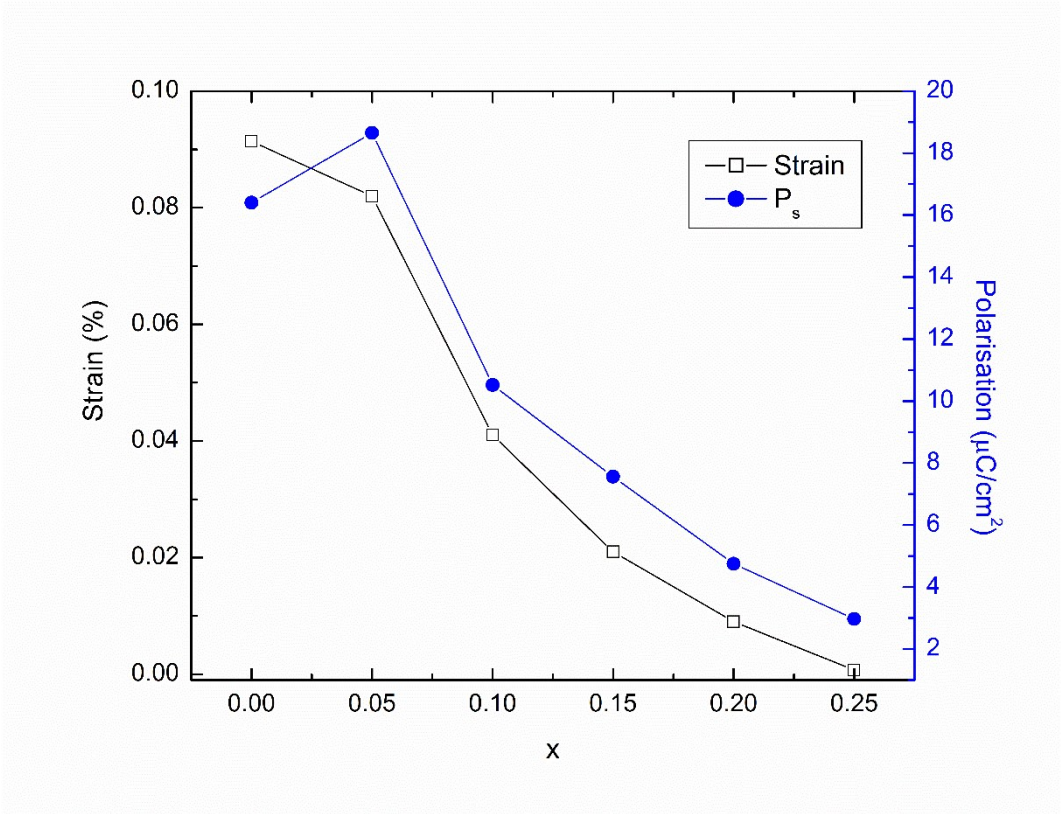

Figure S9. Compositional variation of the electric field-induced strain and of the spontaneous polarisation for KN-BBNZ ceramics measured at 80 kV/cm and 1 Hz.

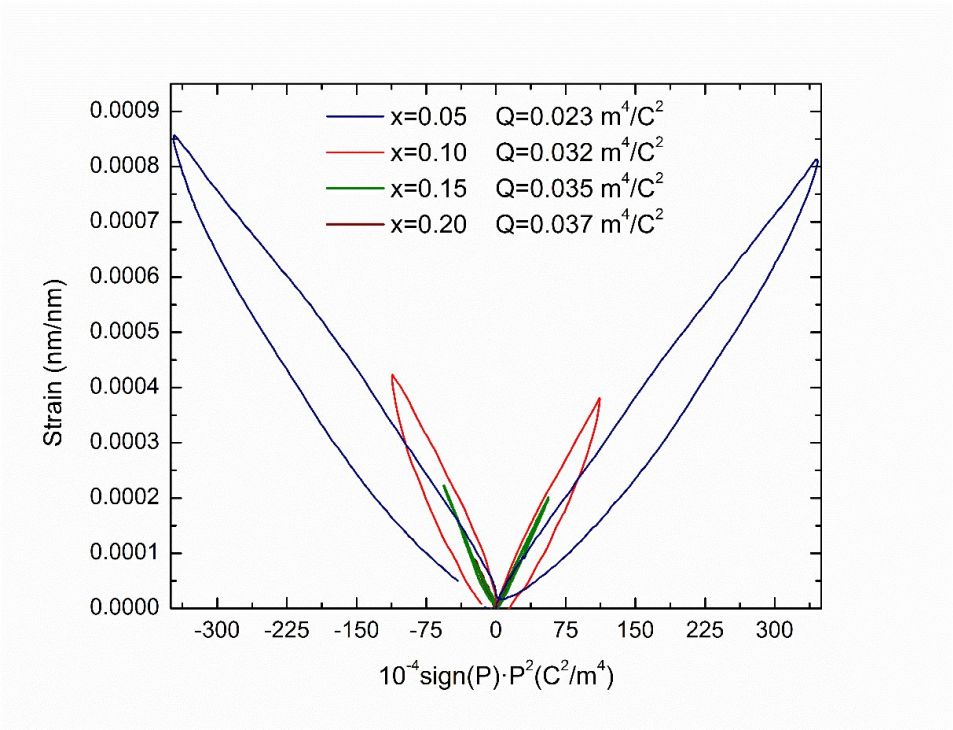

Figure S10. Strain versus Squared Polarisation for KN-BBNZ x=0.05-0.20 used to calculate electrostrictive coefficients, Q.

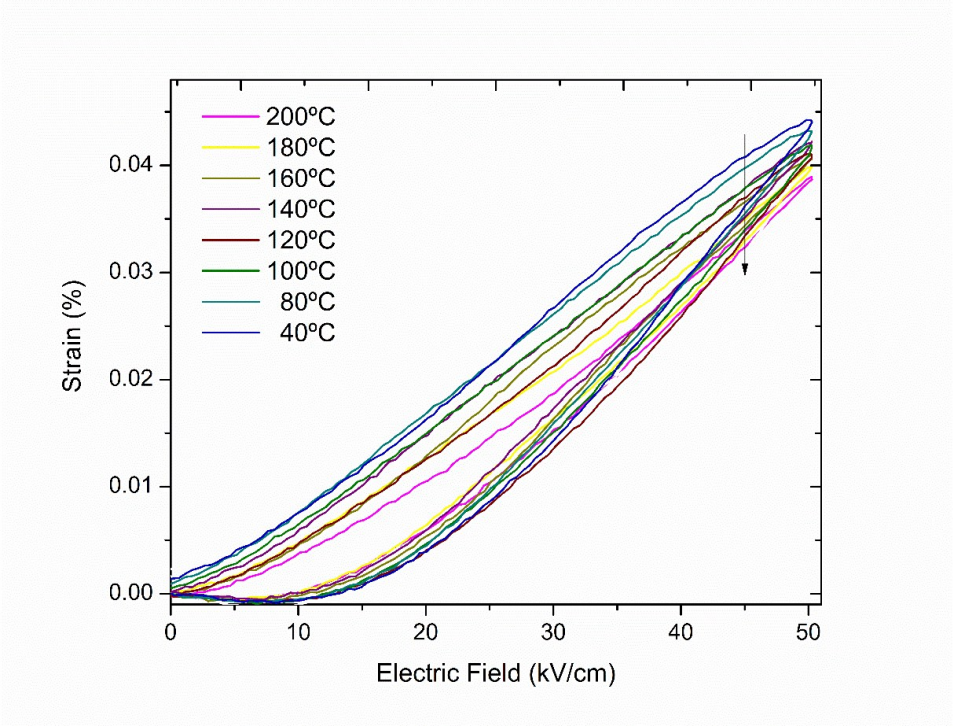

Figure S11. Temperature dependence of the unipolar electric field-induced strain (measured at 50 kV/cm) for KN-BBNZ x=0.05 ceramics, shows a moderate variation of ~13% from 40 to 200℃. Arrow indicates increasing temperature.

	x=0	x=0.05	x=0.10		x=0.15		x=0.2	x=0.25
Space Group	Amm2	Amm2	71.8(4)% Amm2	28(1)% $Pm\bar{3}m$	28.5(3)% Amm2	71.5(6)% $Pm\bar{3}m$	$Pm\bar{3}m$	$Pm\bar{3}m$
Density (Experimental) (g/cm^3)	4.35(16)	4.42(11)	4.86(6)		4.96(8)		4.42(11)	5.24(13)
Density (calculated) (g/cm^3)	4.6280(2)	4.6523(4)	4.8956(1)	4.9063(2)	5.051(3)	5.036(3)	5.186(3)	5.3168(2)
Relative Density (%)	94(3)	95(2)	97(0.5)	97(0.5)	96(1)	97(1)	96(2)	98 (2)
a (Å)	3.9708(1)	4.0057(1)	4.0266(1)	4.0204(1)	4.0399(6)	4.0268(1)	4.0276(1)	4.0331(1)
b (Å)	5.6932(1)	5.6763(3)	5.6927(1)	4.0204(1)	5.6730(20)	4.0268(1)	4.0276(1)	4.0331(1)
c (Å)	5.7129(1)	5.6935(3)	5.6822(1)	4.0204(1)	5.6810(20)	4.0268(1)	4.0276(1)	4.0331(1)
$V/10^6$ (pm^3)								

	64.576(2)	64.729(5)	65.128(3)	64.983(3)	65.100(3)	65.294(3)	65.334(4)	65.602(3)
Rexp	1.44820	1.45269	1.45707		1.44527		1.44843	1.23751
Rprofile	3.47520	2.31942	2.03994		2.18202		2.40865	1.47899
Rwp	5.75210	3.29451	2.95423		2.75964		3.17362	4.44817
GOF	15.83085	5.14322	4.11080		3.64964		4.80078	9.04555
R (Bragg)	---	---	1.46526	1.37490	1.01167	0.99093	---	---

Table I. Relative densities and lattice metrics for KN-BBNZ ceramics.

KN-BBZN	**x=0**	**x=0.05**	**x=0.10**	**x=0.15**	**x=0.20**	**x=0.25**
$E_g^{Indirect}\ (eV)$	3.22	2.96	3.06	3.03	2.99	2.89

Table II. Indirect band gaps for KN-BBZN ceramics.